

# Saturation of Zeldovich Stretch-Twist-Fold Map Dynamos

AMIT SETA<sup>1,2†</sup>, PALLAVI BHAT<sup>3</sup>  
AND KANDASWAMY SUBRAMANIAN<sup>3</sup>

<sup>1</sup>UM-DAE Center For Excellence in Basic Sciences, University of Mumbai, Vidhyanagari Campus, Mumbai 400098, India

<sup>2</sup>School of Mathematics & Statistics, Newcastle University, Newcastle upon Tyne NE1 7RU, UK.

<sup>3</sup>IUCAA, Post Bag 4, Ganeshkhind, Pune 411 007, India.

(Received 19 March 2019)

Zeldovich’s stretch-twist fold (STF) dynamo provided a breakthrough in conceptual understanding of fast dynamos, including fluctuation or the small scale dynamos. We study the evolution and saturation behaviour of two types of generalized Baker’s map dynamos, which have been used to model Zeldovich’s STF dynamo process. Using such maps allows one to analyze dynamos at much higher magnetic Reynolds numbers  $R_M$  as compared to direct numerical simulations. In the 2-strip map dynamo there is constant constructive folding while the 4-strip map dynamo also allows the possibility of reversal of the field. Incorporating a diffusive step parameterised by  $R_M$  in to the map, we find that the magnetic field  $B(x)$  is amplified only above a critical  $R_M = R_{\text{crit}} \sim 4$  for both types of dynamos. The growing  $B(x)$  approaches a shape invariant eigenfunction, whose fine structure increases with increasing  $R_M$ . We explore the saturation of these dynamos in three ways; by a renormalized decrease of the effective  $R_M$  (Case I) or due to a decrease in the efficiency of field amplification by stretching (Case II), or a combination of both effects (Case III). For Case I, we show that  $B(x)$  in the saturated state, for both types of maps, goes back to the marginal eigenfunction, which is obtained for the critical  $R_M = R_{\text{crit}}$ . This is independent of the initial  $R_M = R_{M0}$ . On the other hand in Case II, for the 2-strip map, we show that  $B(x)$  now saturates preserving the structure of the kinematic eigenfunction. Thus the energy is transferred to larger scales in Case I but remains at the smallest resistive scales in Case II. For the 4-strip map, the  $B(x)$  oscillates with time, although with a structure similar to the kinematic eigenfunction. Interestingly, the saturated state for Case III shows an intermediate behaviour, with  $B(x)$  now similar to the kinematic eigenfunction for an intermediate  $R_M = R_{\text{sat}}$ , with  $R_{M0} > R_{\text{sat}} > R_{\text{crit}}$ .  $R_{\text{sat}}$  is determined by the relative importance of the increased diffusion versus the reduced stretching. These saturation properties are akin to the range of possibilities that have been discussed in the context of fluctuation dynamos.

## 1. Introduction

Magnetic fields in astrophysical systems are thought to arise by amplification of a seed magnetic field by dynamo action. In this process kinetic energy of motions is converted to magnetic energy. A generic dynamo is the small-scale or fluctuation dynamo, which arises in any random or turbulent flow (Kazantsev 1968; Zeldovich *et al.* 1983; Haugen *et al.* 2004; Schekochihin *et al.* 2004; Brandenburg & Subramanian 2005;

† Email address for correspondence: amitseta90@gmail.com

Tobias *et al.* 2011; Brandenburg *et al.* 2012; Bhat & Subramanian 2014). It is well known that when magnetic Reynolds number  $R_M$ , of such a flow is above a certain critical threshold  $R_{\text{crit}} \sim 100$ , the magnetic field in the fluid is amplified rapidly on the eddy turn over time-scales of the flow. This amplification is due to the random stretching by the velocity shear of the turbulent flow. Such shearing motions also lead to the magnetic field developing smaller and smaller spatial scales, until resistive diffusion becomes important to balance the growth. The field then becomes highly intermittent with the kinematic eigenfunction having power peaked on the resistive scales (Kazantsev 1968). For a random flow driven on a (single) scale  $l$ , the resistive scale is  $l_\eta \sim l/R_M^{1/2}$ , and for  $R_M \gg 1$ , it is much smaller than the driving scale  $l$ . Eventually Lorentz forces of the growing magnetic field provides a back reaction to the dynamo action, leading to saturation of magnetic field growth. The nature and spatial coherence of the field in the saturated state is of paramount importance to the observational signatures of this field in different astrophysical systems (Subramanian *et al.* 2006; Enßlin & Vogt 2006; Schekochihin & Cowley 2006; Bhat & Subramanian 2013), but is however not well understood at present (Brandenburg & Subramanian 2005; Tobias *et al.* 2011; Brandenburg *et al.* 2012).

Indeed there is considerable evidence for coherent magnetic fields in several systems like galaxy clusters (Clarke *et al.* 2001; Clarke 2004) and in young galaxies (Bernet *et al.* 2008) from observations of Faraday rotation that these systems induce on background polarized sources. A possible origin of these fields is fluctuation dynamo action. However, whether one can indeed reproduce the observed levels of Faraday rotation measure (FRM) depends on the spatial coherence of the fields produced by fluctuation dynamo. As these systems have typically  $R_M \gg 1$ , the field needs to become much more coherent at the saturated state than it is at the kinematic stage for it to explain the observations (Bhat & Subramanian 2013).

The saturation of fluctuation dynamos has been studied both via direct numerical simulations (DNS) and some simple analytical models. A simple model of Subramanian (1999) suggests that the dynamo can saturate by Lorentz forces driving the dynamo to its marginal state. In such a case the magnetic field in the saturated state concentrates on scales  $l_c \sim l/R_{\text{crit}}^{1/2}$ . As  $R_{\text{crit}} \ll R_M$  typically, this implies a much more coherent field in the saturated state of the dynamo than during the kinematic stage. Using DNS with large magnetic Prandtl numbers ( $P_M = R_M/\text{Re} \gg 1$ ), but small fluid Reynolds numbers ( $\text{Re}$ ), Schekochihin *et al.* (2004) argued that the fluctuation dynamo generated fields saturate with the magnetic field still concentrating on resistive scales. On other hand simulations of Haugen *et al.* (2003, 2004) and Eyink *et al.* (2013) with  $P_M = 1$  and a large  $R_M = \text{Re} \approx 10^3$ , found the magnetic integral scale is just a modest fraction of the velocity integral scale, and much larger than the resistive scale. One could then expect significant FRMs, as is also consistent with the theoretical expectation from Subramanian (1999) and the DNS results of Subramanian *et al.* (2006); Cho & Ryu (2009); Bhat & Subramanian (2013). The case when both  $\text{Re}$  and  $P_M$  are large, as in galactic and cluster plasmas, is of course not easy to simulate and the saturation of the fluctuation dynamo could be quite different (Eyink 2011).

Note that DNS are limited by the  $R_M$  that are achievable and still perhaps do not have a large enough  $R_M$  to unambiguously determine the saturated state. At the same time the analytical models are still rather simplistic. In this context one may wonder if there is any other independent and simple way of studying the generic saturation properties of fluctuation dynamos. We consider here map dynamos that have been studied earlier in the literature to mimic kinematic fast dynamo action, and examine how such maps could

saturate. Such map dynamos typically lead to a fractal structure of the field, where the field goes into smaller and smaller scales (Finn & Ott 1988, 1990; Childress & Gilbert 1995). However with the incorporation of a diffusive step in the map, they can lead to eigenfunctions which preserve their shape, and have the smallest scale determined by the resistivity (or the effective  $R_M$ ). In the case of such map dynamos one can reach much larger  $R_M$  than for the case of DNS. We then examine simple models of saturating the map dynamo and study how the spatial structure of the map eigenfunction changes from the kinematic to the saturated state. Our aim is then to get insight in to some generic properties of the saturated states of the fluctuation dynamo itself.

In the next section we begin with the description of the standard Stretch-Twist-Fold (STF) dynamo (Vainshtein & Zel'dovich 1972). The corresponding map model for the STF dynamo is outlined in section 3. Results from numerical simulation of the STF map dynamo for various  $R_M$  is given in section 4. The saturation of the STF map dynamos is taken up in section 5. The last section presents a discussion of the results and our conclusions.

## 2. Zeldovich's STF dynamo

To explain the possibility of the fast dynamos i.e. growth of magnetic field even when resistivity goes to zero, Vainshtein & Zel'dovich (1972) put forward a heuristic description referred to as 'Stretch-Twist-Fold' (STF) dynamo. The algorithm involves first stretching a closed flux tube to double its length (see for example Fig. 4.6 in Brandenburg & Subramanian (2005)) preserving its volume (a characteristic of an incompressible flow). Assuming flux to be frozen in the flux tube, the magnetic field doubles as area of cross-section goes down by a factor of two. Next, the flux tube is twisted into a figure eight and then folded systematically so the direction of magnetic field is same in both the sub-parts. Then the both the parts are merged together into one through small diffusive effects to occupy the same volume as the starting point. A weak diffusion is thus required to make the process of merging irreversible by smoothing region between the two flux tubes during joining without much loss in the flux or energy. It may thus be more appropriate to refer to this process as the Stretch-Twist-Fold-Merge dynamo, although we continue with the standard terminology here.

Hence, the final flux tube becomes equivalent to the original single flux tube, but with a field that is double the initial field. It is important to mark the way the two parts are folded, if they are folded with fields pointing in opposite directions it would lead to cancellation of field and can depict the field reversals due to turbulence in the actual physical situation. For constructive folding, with each step the flux and thus the magnetic field increases by a factor of 2, repeating the same process  $n$  times the magnetic field increases by a factor of  $2^n$ . Thus the growth rate is  $\sim T^{-1} \ln 2$  where  $T$  is the time for one STF step. The stretching can also be done in a non-uniform manner. Suppose the stretching is done non-uniformly, by stretching a fraction  $\beta$  (where  $0 < \beta < 1/2$ ) of the circumference ( $2\pi R$ ) by an amount  $1/\beta$  and  $2\pi\alpha R$  part of the circumference by  $1/\alpha$  (where  $\alpha = 1 - \beta$ ). Then this would give rise to same increment in magnetic field as before but in a non-uniform way. Repeated operation of the STF process on such an inhomogeneous flux tube or on one that has developed reversals, would lead to the magnetic field developing a fine scale structure that can mimic the intermittent nature of the field generated by fluctuating dynamos.

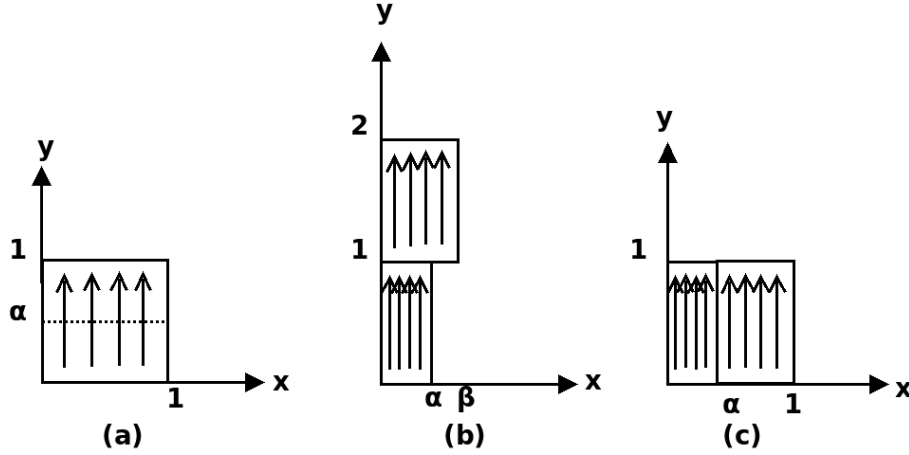


FIGURE 1. The two-dimensional Baker's map as a model for the stretch-twist-fold dynamo, but with non-uniform stretching.

### 3. Map Models for Zeldovich's STF Dynamoes

Finn & Ott (1988, 1990) studied a map analogue of Zeldovich's Stretch-Twist-Fold fast dynamo. Fig.3 represents the two-dimensional map which is used to model the dynamo processes. This map is an example of the generalised Baker's map (Childress & Gilbert 1995). We begin with a perfectly conducting two dimensional square sheet in the  $x - y$  plane, and a uniform upward (or  $y$ ) directed seed magnetic field of say a unit strength. The magnetic field initially, and at all times is independent of  $y$  (analogous to being independent of the toroidal direction in a flux tube). Now, the lower part of the square ( $0 < y < \alpha$ ) is horizontally compressed by a factor  $\alpha$  and to conserve area, the lower part is also stretched vertically by factor  $1/\alpha$ . Similarly, the upper part ( $\alpha < y < 1$ ) is compressed by factor  $\beta$  (along  $x$ ) and stretched by factor  $1/\beta$  (along  $y$ ) where  $\beta = 1 - \alpha$ . Then the two parts are separated and the magnetic field between the two parts is cut and the two pieces are re-arranged to get back the original square. (This non-physical action allows one to describe an inherently three-dimensional physical process by a two-dimensional map; moreover there cannot be any dynamo action in two-dimensional flows (Zeldovich *et al.* 1983)). As the flux is frozen in the region ( $\eta \rightarrow 0$ ), the field through the  $\alpha$  strip,  $B_\alpha$  increases by  $1/\alpha$  and the field through the  $\beta$  strip,  $B_\beta$  by  $1/\beta$ . Then the total flux is  $B_\alpha\alpha + B_\beta\beta = 2$ , and thus the flux through entire square doubles. The average magnetic field also doubles within the square as compared to the initial field.

The equivalent map depicting the above process is as follows:

$$x_{n+1} = \begin{cases} \alpha x_n & : y_n < \alpha \\ \beta x_n + \alpha & : y_n > \alpha \end{cases} \quad (3.1)$$

$$y_{n+1} = \begin{cases} y_n/\alpha & : y_n < \alpha \\ (y_n - \alpha)/\beta & : y_n > \alpha \end{cases} \quad (3.2)$$

Note that  $x_n$  and  $y_n$  take values in the interval  $[0, 1]$ . The corresponding amplification of magnetic field in the region is given as follows:

$$B_{n+1}(x_{n+1}) = \begin{cases} B_n(x_n)/\alpha & : x_n < \alpha \\ B_n(x_n)/\beta & : x_n > \alpha \end{cases} \quad (3.3)$$

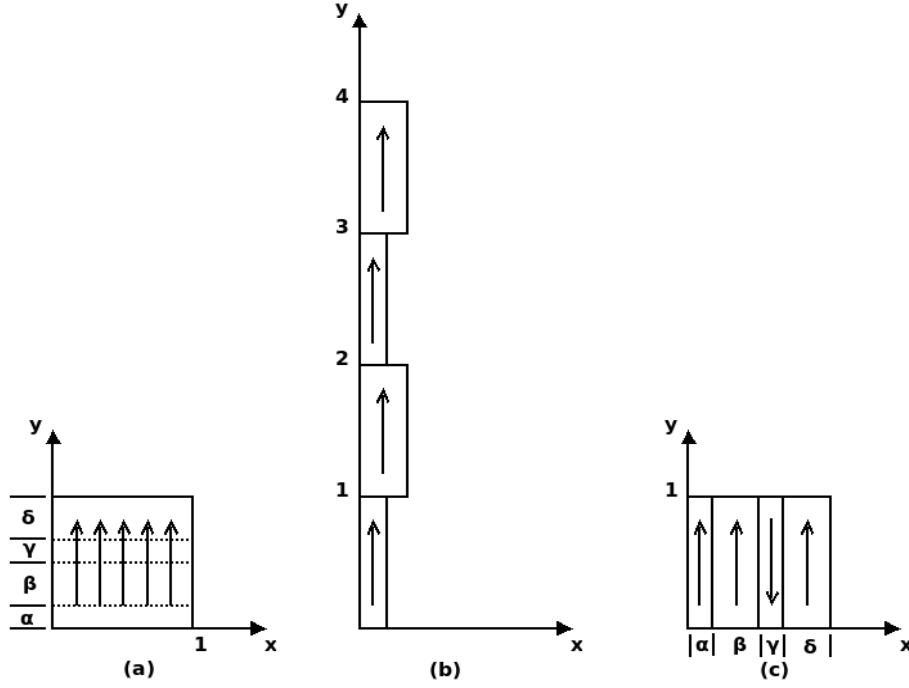


FIGURE 2. The two-dimensional 4-strip Baker's map as a model for the stretch-twist-fold dynamo with cancellation of fields.

### 3.1. Amplification, Cancellation and 4-strip map

To include field reversals, which are an important part of the physical dynamo process leading to cancellation of magnetic fields, Finn & Ott (1988, 1990) suggest a different model for STF dynamos. The flux tube in this case is stretched non-uniformly to four times its original circumference, twisted in to four loops, and two of the loops are folded with same orientation of magnetic field while the other two with opposite directions of fields thus leading to field cancellation. The corresponding map is shown in Fig.2. The net field increase is same as the 2-strip map, the field doubles with each step. As shown in the Fig.2, the analogous map would involve dividing the square into four strips and while rearranging the strips, one of them is inverted and then placed to regain the initial square configuration. The analytical description of the four strip map is given by,

$$x_{n+1} = \begin{cases} \alpha x_n & : y_n < \alpha \\ \beta x_n + \alpha & : \alpha < y_n < (\alpha + \beta) \\ \gamma(1 - x_n) + \alpha + \beta & : (\alpha + \beta) < y_n < (\alpha + \beta + \gamma) \\ \delta x_n + \alpha + \beta + \gamma & : (\alpha + \beta + \gamma) < y_n < 1 \end{cases} \quad (3.4)$$

$$y_{n+1} = \begin{cases} y_n/\alpha & : y_n < \alpha \\ (y_n - \alpha)/\beta & : \alpha < y_n < (\alpha + \beta) \\ ((\alpha + \beta + \gamma) - y_n)/\gamma & : (\alpha + \beta) < y_n < (\alpha + \beta + \gamma) \\ (y_n - (\alpha + \beta + \gamma))/\delta & : (\alpha + \beta + \gamma) < y_n < 1 \end{cases} \quad (3.5)$$

Again  $x_n$  and  $y_n$  take values in the interval  $[0, 1]$ . The corresponding amplification of magnetic field with a flip of sign in the third strip is now given by:

$$B_{n+1}(x_{n+1}) = \begin{cases} B_n(x_n)/\alpha & : y_n < \alpha \\ B_n(x_n)/\beta & : \alpha < y_n < (\alpha + \beta) \\ -B_n(x_n)/\gamma & : (\alpha + \beta) < y_n < (\alpha + \beta + \gamma) \\ B_n(x_n)/\delta & : (\alpha + \beta + \gamma) < y_n < 1 \end{cases} \quad (3.6)$$

We will study both 2-strip and 4-strip maps in what follows.

### 3.2. Including Diffusion

As discussed above, it is important to include the smoothing effects of diffusion in the STF dynamo. We do this in the maps by convolving the evolved magnetic field after each step with a Gaussian. If  $T$  is the time interval for each complete cycle of the STF map, the assumption is that for the time  $T/2$  the diffusive term in the induction equation can be neglected, the flux is frozen and the field amplifies. For the remaining period,  $T/2$ , the advection term goes to zero and pure diffusion acts, with twice the normal diffusivity. The magnetic Reynolds number  $R_M$  is the measure of advection in comparison to diffusion and thus should be a parameter in the convolving function. The convolving Gaussian (also the Greens function for diffusion) is therefore taken as (Finn & Ott 1990),

$$G(x, x') = (R_M/4\pi T)^{1/2} \exp[-(x - x')^2(R_M/4T)]. \quad (3.7)$$

The width of the Gaussian ( $\sigma = \sqrt{2T/R_M}$ ) is inversely proportional to the  $\sqrt{R_M}$  and shows that the diffusion goes down when  $R_M$  increases and vice-versa. A single iteration involves applying the map to amplify the magnetic field and then convolving the evolved field with a Gaussian for the diffusion.

## 4. Results: Kinematic Stage

We have coded the amplification of the magnetic field using maps given in Eq. 3.1 - 3.6 and also included diffusion using the set of points generated by map itself. The distribution of points in the interval  $[0, 1]$  is dynamic and the map automatically allocates more number of points to areas where the magnetic field has finer structure, this allows us to achieve higher  $R_M$  than the number of points that are used. We have generally adopted  $300 \times 300$  for lower  $R_M$  runs while for higher  $R_M$  we use  $500 \times 500$  points.

We first show in Fig. 3, the result of applying the 2 strip map, excluding diffusion step to look at kinematic evolution of magnetic field starting from a unit seed field. The panels in Fig. 3 from top to bottom show respectively, the magnetic field  $B(x)$ , as a function of position  $x$ , after 1, 2, 4 and 8 iterations. We have adopted here  $\alpha = 0.4$ . It is clear from Fig. 3 that as the number of iterations increases the magnetic field grows but becomes more and more intermittent. Moreover, within a small spatial scale the magnetic field varies significantly and develops a fractal structure (Finn & Ott 1988, 1990).

### 4.1. Critical magnetic Reynolds number

On including diffusion, the process of amplification has to win over the diffusion for net amplification to occur. This introduces a concept of critical  $R_M = R_{\text{crit}}$ , only above which net amplification takes place. We show in Fig. 4 (left panel) that starting with an initial seed field of 1,  $B(x)$  does not get amplified till a critical  $R_M$  is reached. The critical magnetic Reynolds number for the 2 strip map turns out to be,  $R_{\text{crit}} \approx 4.35$ .

We have also repeated the same process for the 4-strip map with cancellation adopting  $\alpha = \delta = 7/16$  and  $\beta = \gamma = 1/16$ . The results which are shown in Fig. 4 (right panel)

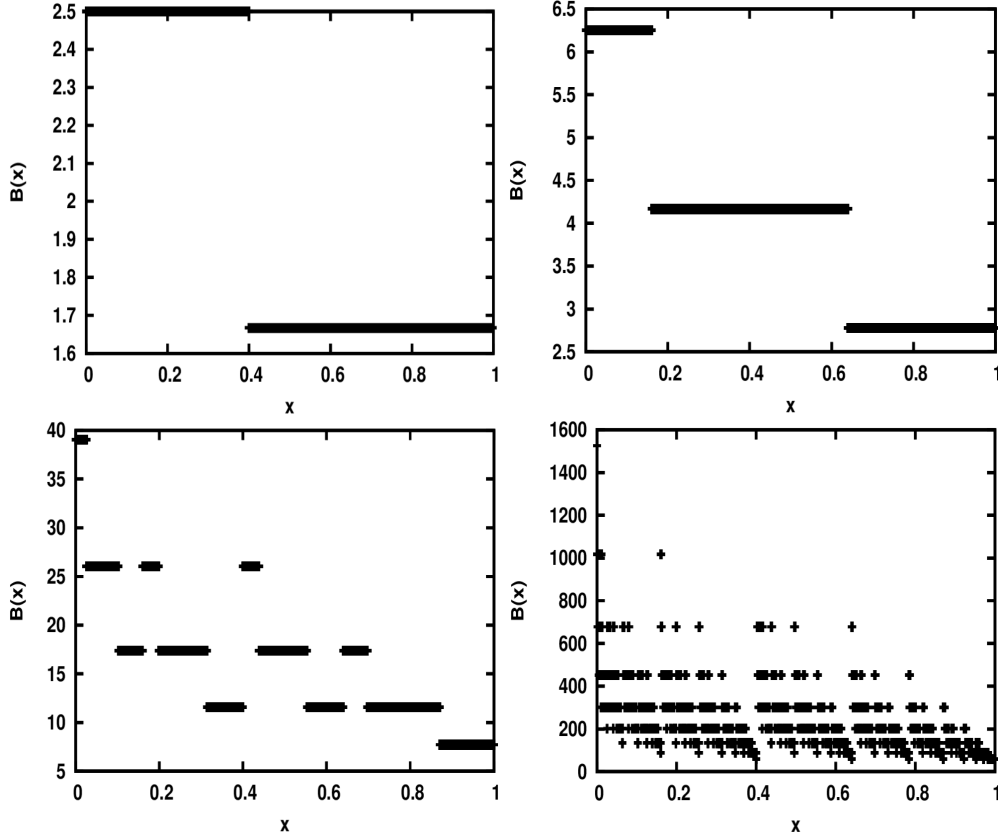


FIGURE 3. Magnetic field evolution in the 2-strip map with  $\alpha = 0.4$  after 1, 2, 4 and 8 iterations (top to bottom panels). The magnetic field strength  $B(x)$  in units of the seed field. We see the amplification of the field strength and development of the intermittent structure of the field as the number of iterations increase.

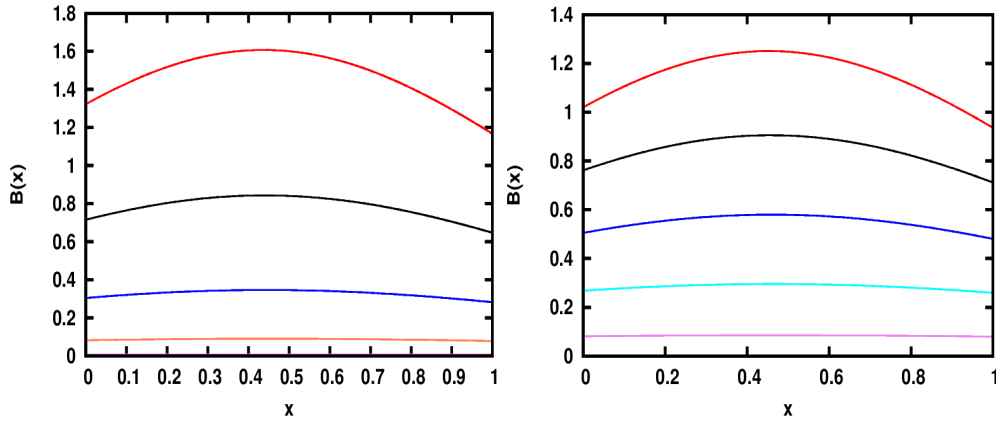


FIGURE 4.  $B(x)$  for 2-strip map (left panel) and for the 4-strip map (right panel) including diffusion after 8 iterations. In the left panel the curves from bottom to the top correspond to values of  $R_M = 2, 3, 4, 5$  respectively, while in the right panel they correspond to  $R_M = 1, 2, 3, 4, 5$ . The field is amplified for a critical magnetic Reynolds number  $R_{\text{crit}} \gtrsim 4$  in both cases.

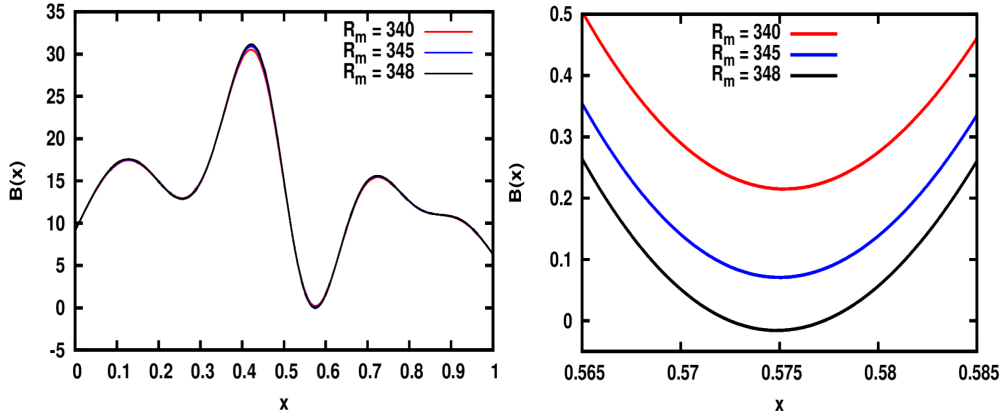


FIGURE 5.  $B(x)$  for the 4-strip map after 4 iterations, with the darker curve corresponding to a larger  $R_M$ . A magnified version is shown in the lower panel.  $B(x)$  becomes negative first for  $R_M \sim 348$ , dependent on stretching parameters. Here we have adopted  $\alpha = \delta = 7/16$  and  $\beta = \gamma = 1/16$ .

indicates a critical magnetic Reynolds number which is very close to that obtained for the 2-strip map.

It is interesting to note that in the 4-strip map, though there is an amplification in negative direction, there is no field with negative polarity till a large enough  $R_M$  is reached. This critical  $R_M$  of course depends on stretching parameters, in particular the value of  $\gamma$ , which determines the degree of amplification in the negative direction. As seen in Fig. 5, the field in the region has negative polarity solutions only for  $R_M \gtrsim 348$  for parameters,  $\alpha = \delta = 7/16$  and  $\beta = \gamma = 1/16$ .

#### 4.2. Eigenfunctions of the map dynamo

After a few iterations, the function  $B(x)$  representing variation of magnetic field along  $x$  settles to an eigenfunction of a specific shape and  $B(x)$  from future iterations can be matched to it by scaling. This can be seen in Fig. 6 for a 2-strip map. For example the function  $B(x)$  after the 7th iteration can be scaled back in amplitude to  $B(x)$  after 6th iteration. Thus  $B(x)$  latches on to an eigenfunction of the map system with diffusion included (which represents the STF dynamos). These eigenfunctions for the two strip map depend of course on  $R_M$ . This is clear from Fig. 7, where we see that with increasing  $R_M$  (from  $10^2$  to  $10^5$ ), the eigenfunction of the magnetic field develops a finer and finer scale structure. It can be seen that the eigenfunctions in Fig. 7 for different  $R_M$  match with those in Fig. 6 of Finn & Ott (1990), for the same  $\alpha = 0.4$ .

Eigenfunctions for the four strip map with various  $R_M$  ranging from  $10^2$  to  $10^5$  are shown in Fig. 8. As  $R_M$  is increased beside showing features similar to the 2 strip maps, there also exists fine scale reversals between the parallel and anti-parallel direction of the magnetic fields. These could be thought of as the analogue of the field reversals seen in DNS of fluctuation dynamos (Schekochihin *et al.* 2004; Brandenburg & Subramanian 2005). We now turn to the saturation of STF type map dynamos.

## 5. Saturation of STF map dynamos

Saturation of dynamos can occur in several different ways. Possibilities include the normalization and increase of the effective resistivity due to Lorentz forces (Subramanian 1999) or the decreased stretching efficiency (Schekochihin *et al.* 2004). We model these

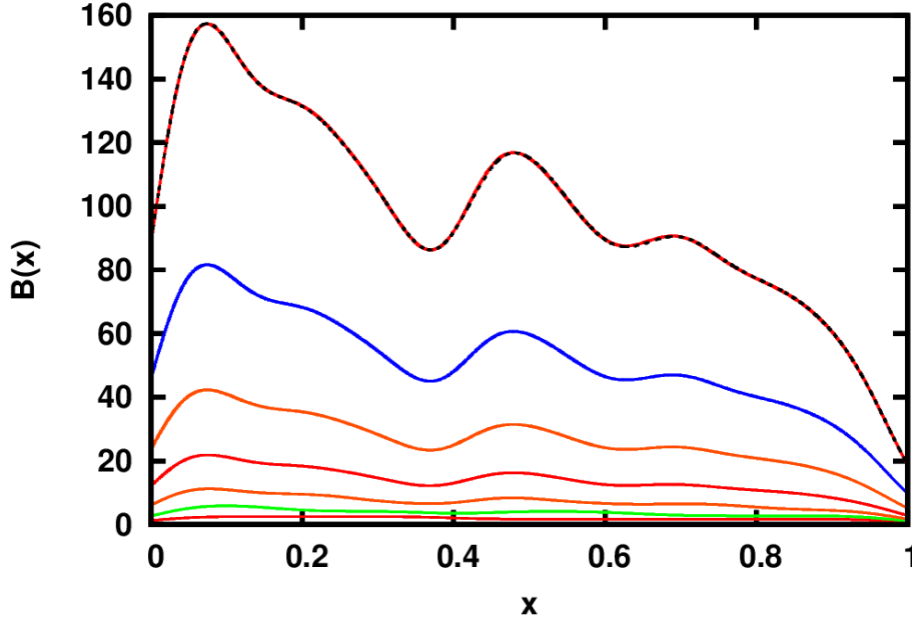


FIGURE 6.  $B(x)$  for the 2-strip map for iterations 1 to 7 (from bottom to top), adopting  $\alpha = 0.4$  and  $R_M = 1000$ .  $B(x)$  after the 7th iteration is just a scaled version of  $B(x)$  after the 6th iteration illustrating the build up of the map eigenfunction.

in simple ways below to study the saturation of the map dynamos. We will now set the absolute value of the saturated magnetic field strength to be of order unity, and therefore start with an initial seed field of  $10^{-4}$ .

### 5.1. Saturation by decreasing $R_M$

As one possibility consider saturating the dynamo by varying  $R_M$  every iteration as,

$$R_M = \frac{R_{M0}}{1 + R_{M0}(B_{rms}^2)}, \quad (5.1)$$

where  $R_{M0}$  is the initial value of  $R_M$  and  $B_{rms}^2$  is the average value of  $B^2(x)$  at any iteration (or time). This form models the possible increase of the renormalized resistivity due to Lorentz forces.

The time evolution of  $B(x)$  is shown in the left and right panels of Fig. 9 for  $R_{M0} = 1000$  and  $R_{M0} = 10^4$  respectively. The evolution of corresponding  $B_{rms}$  is shown in Fig. 14 as case (a) and case (b) respectively. We see from Fig. 14 that  $B_{rms}$  indeed saturates after about 7 – 10 iterations, to a value of order unity. Moreover, comparing Fig. 9 with Fig. 4, it is clear that the function  $B(x)$  representing the saturated state, is of the same form as  $B(x)$  for the critical  $R_M$  ( $\sim 4.35$ ). Further in the saturated stage the  $R_M$  given by the Eq. 5.1, also settles to  $R_{sat} = R_{crit} \sim 4$ , using  $B_{rms} \sim 0.5$  and  $R_{M0} = 1000$ .

Employing a similar method of saturation for the 4-strip map with cancellation adopting an initial  $R_M = 10^5$  also gives similar results as shown in Fig. 10. The corresponding evolution of  $B_{rms}$ , case (c) in Fig. 14, shows that  $B_{rms}$  saturates again after about ten iterations, to a value of order unity. Again comparing eigenfunctions  $B(x)$  in Fig. 10 with Fig. 4 (right panel), it is clear that the saturated eigenfunction is equivalent to

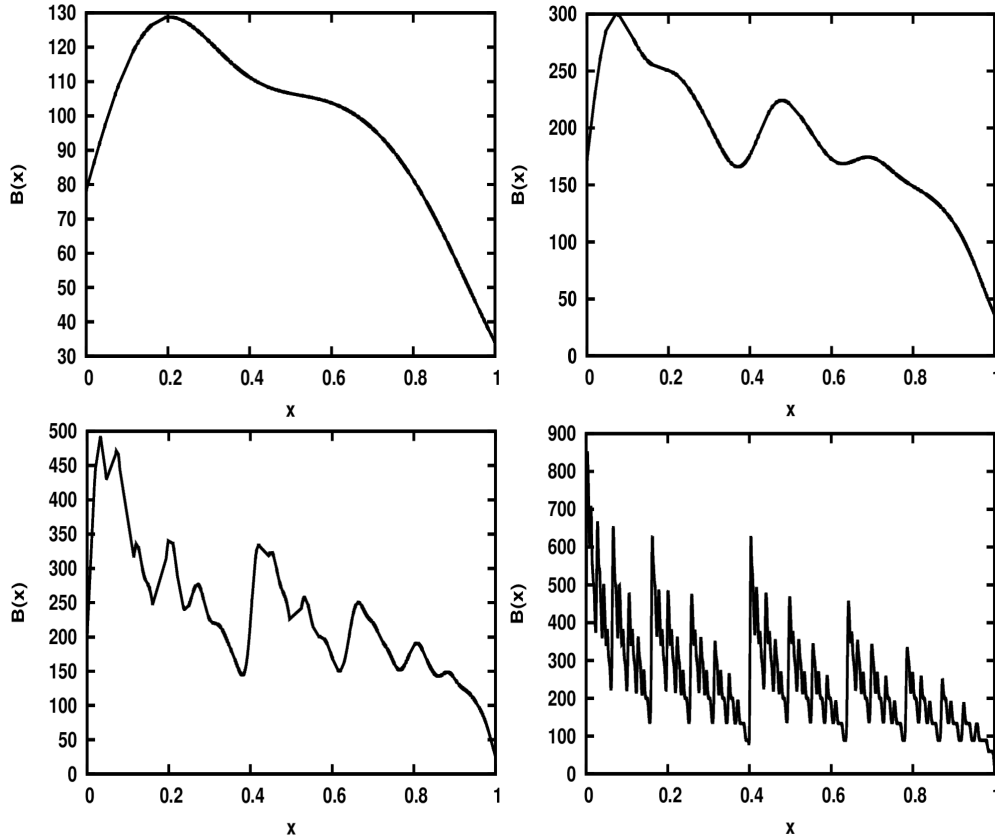


FIGURE 7. Eigenfunctions for the 2-strip map with  $\alpha = 0.4$  and for  $R_M = 100, 1000, 10^4, 10^5$  (top to bottom panels).

the marginal eigenfunction which is obtained for the critical magnetic Reynolds number, with  $R_{\text{sat}} = R_{\text{crit}} \sim 4.35$ .

Thus in the case where saturation is obtained by renormalization of  $R_M$ , we find that the saturated state has the same spatial structure as the marginal state of the kinematic map dynamo. Such a result is similar to the saturation behaviour obtained in Subramanian (1999) and perhaps in the simulations of Haugen *et al.* (2004) for the  $P_M = 1$  fluctuation dynamo.

### 5.2. Saturation by decreasing stretching

As the magnetic field strength increases, the effect of the Lorentz force would be to make it more difficult to amplify the field by stretching. Therefore, another way to achieve saturation in the maps would be to decrease the field amplification factor  $\propto 1/\alpha$  as a function of  $B_{\text{rms}}$ . We model this effect by multiplying  $\alpha, \beta$  in Eq. 3.3 for the 2-strip map and  $\alpha, \beta, \gamma, \delta$  in Eq. 3.6 for the 4-strip map by  $(1 + B_{\text{rms}}^2)$ . For example we adopt

$$\alpha = \alpha_0(1 + B_{\text{rms}}^2), \quad (5.2)$$

where  $\alpha_0$  is the initial value of  $\alpha$ . Note that we still leave the mapping of  $(x_n, y_n) \rightarrow (x_{n+1}, y_{n+1})$  described by Eqs. 3.1, 3.2, 3.4 and 3.5 as before, described by the initial  $\alpha_0, \beta_0, \gamma_0$  and  $\delta_0$ . Thus the unit square in the  $x - y$  plane is still mapped to the unit square,

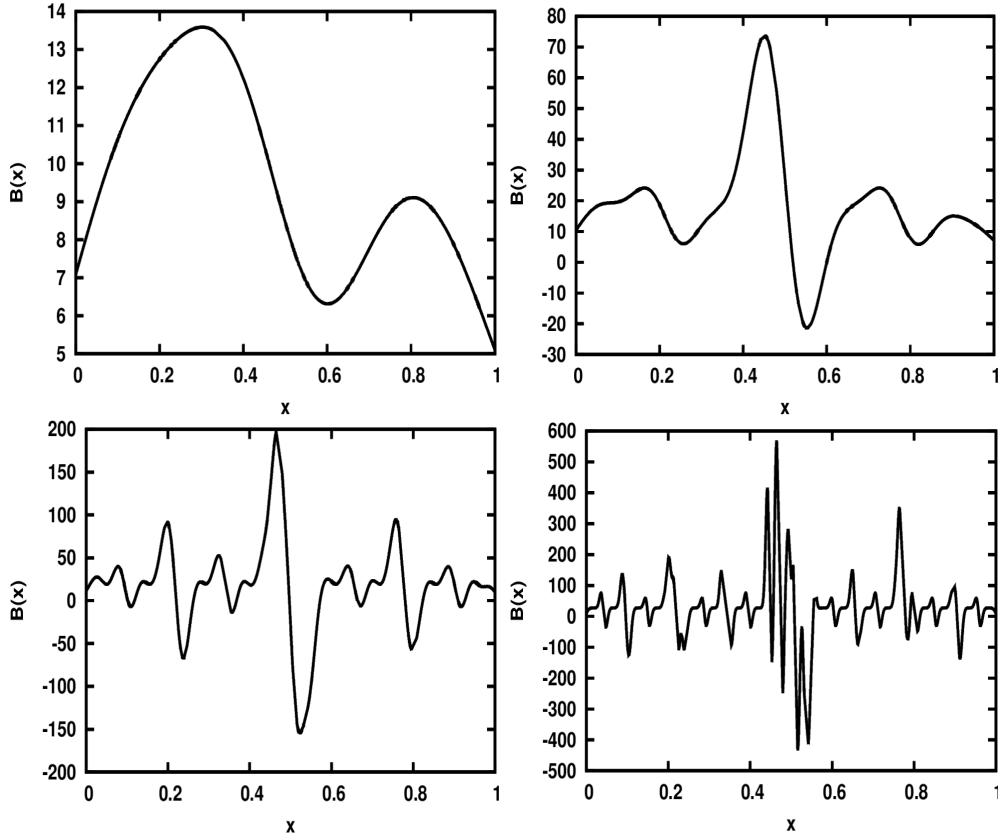


FIGURE 8. Eigenfunctions for the 4-strip map for  $R_M = 100, 1000, 10^4, 10^5$  (top to bottom panels). We have adopted  $\alpha = \delta = 7/16$  and  $\beta = \gamma = 1/16$ .

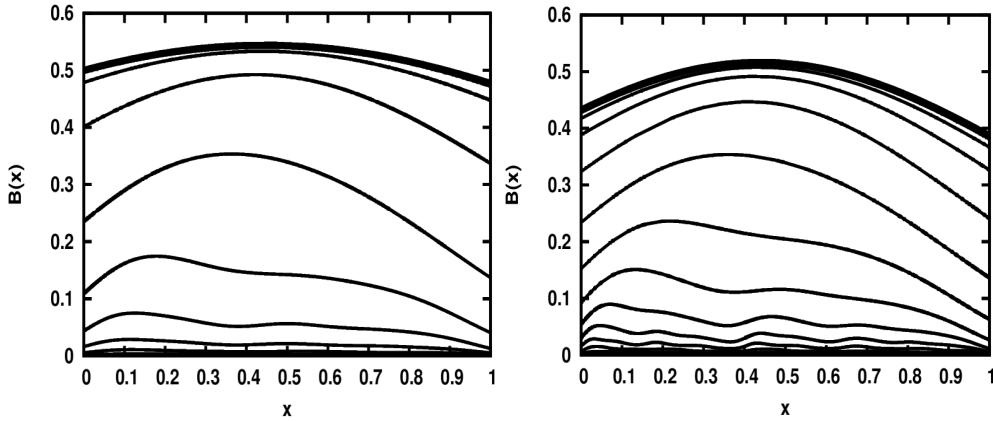


FIGURE 9. The nonlinear evolution of the eigenfunctions of the 2-strip map, due to saturation by increasing resistivity, adopting  $\alpha = 0.4$  and initial  $R_M = 1000$  (left panel) and  $R_M = 10^4$  (right panel). We see that the eigenfunction is driven to that of the marginal eigenfunction corresponding to  $R_M = R_{\text{crit}}$  on saturation.

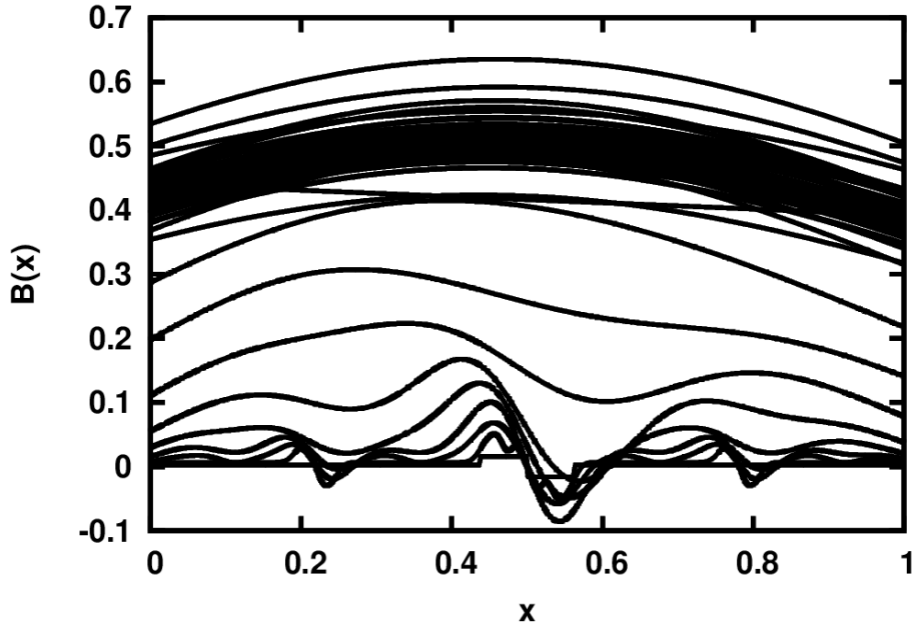


FIGURE 10. Same as in Fig. 9 but for the 4-strip map and  $\alpha = \delta = 7/16$ ,  $\beta = \gamma = 1/16$  and initial  $R_M = 10^5$ . Again the eigenfunction is driven on saturation to the marginal eigenfunction corresponding to  $R_M = R_{\text{crit}}$  of the 4-strip map. on saturation.

but the amplification by stretching becomes progressively inefficient as  $B_{rms}$  grows. † We also now do not change the value of  $R_M$  during the diffusive step.

The result of the such reduced stretching for the 2-strip map is shown in left and right panels of Fig. 11 for  $R_M = 1000$  and  $R_M = 10^4$  respectively. The corresponding  $B_{rms}$  whose evolution is shown in Fig. 14 as cases (d) and (e), saturates after about 10 iterations. It is clear from comparing Fig. 11 with Fig. 7, that the eigenfunction  $B(x)$  representing the saturated state in this case retains the complex structure of the kinematic eigenfunction and is quite different from the case of saturation by increased resistivity. It is thus not the marginal eigenfunction. This saturation behaviour is similar to what is argued by Schekochihin *et al.* (2004) for the fluctuation dynamo with large  $P_M$ , that the field in the saturated state appears to be qualitatively similar to that in the kinematic stage.

We have also employed a similar scheme for the 4-strip map with  $R_M = 1000$ . The results shown in Fig. 12 indicate a very different saturation behaviour. Now, the saturated eigenfunction  $B(x)$  oscillates with time although its form is similar to kinematic eigenfunction. Also  $B_{rms}$  oscillates about a steady value around unity, as can be seen in Fig. 14 (case (f)). This seems to indicate that if reversals are present, the saturated eigenfunction may never settle to a unique form.

† Note that as one reduces stretching by a factor  $f_0 = 1/(1+B_{rms}^2)$  and applies the STF map to a flux tube, its final radius  $R$  would decrease by  $f_0$  while its cross sectional area  $A$  would increase by  $1/f_0$ . In principle the physical dimensions of the unit square that we use to represent the flux tube would then change accordingly and it will become a rectangle with its  $y$ -dimension (analogous to the length of the flux tube) reduced by  $f_0$  and  $x$  dimension (analogous to the cross sectional area of the flux tube) increased by  $1/f_0$ . However, we are thinking of the unit square used in the map as representing the normalised flux tube radius and the normalised cross-sectional area. It is in this sense that the unit square is mapped onto itself, even though the degree of stretching is reducing with the growth of the field.

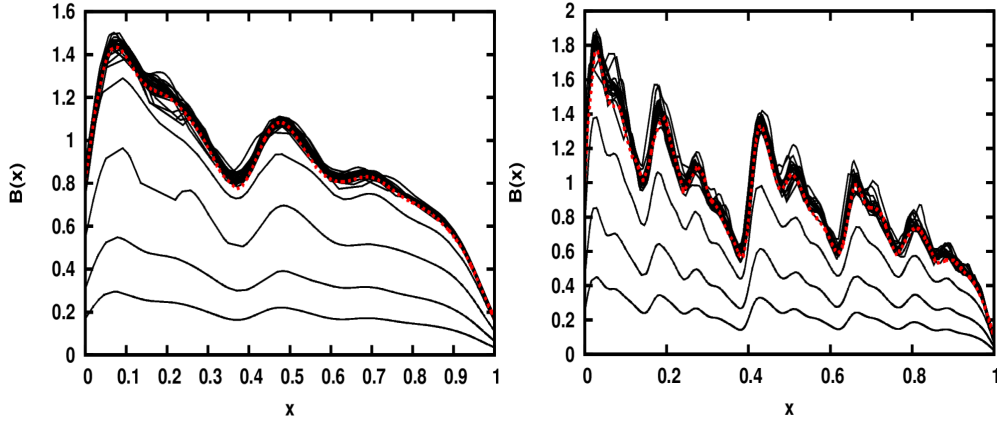


FIGURE 11. The nonlinear evolution of the eigenfunctions of the 2-strip map, due to saturation by reduced stretching, adopting initial  $\alpha_0 = 0.4$  and  $R_M = 1000$  (left panel) and  $R_M = 10^4$  (right panel). The shape of the kinematic eigenfunction for these two cases are shown as dashed (red) lines. We see that the eigenfunction remains similar to the kinematic eigenfunction on saturation.

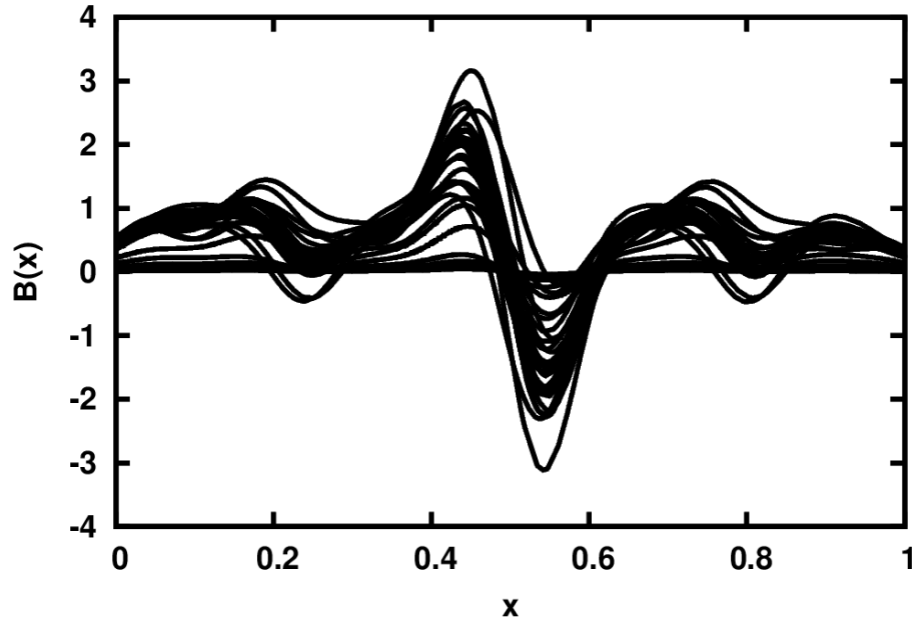


FIGURE 12. Same as in Fig. 11 but now for the 4-strip map adopting an initial  $\alpha_0 = \delta_0 = 7/16, \beta_0 = \gamma_0 = 1/16$  and  $R_M = 1000$ . The eigenfunction on saturation oscillates with a structure similar to the kinematic eigenfunction.

### 5.3. Saturation by combining decreasing both $R_M$ and stretching

We now consider the saturation of the STF map dynamo, when the effects of decreasing effective  $R_M$  (due to increasing renormalised resistivity) and decreasing stretching efficiency are combined. We model this by introducing efficiency parameters  $c_1$  and  $c_2$  into Eqs. 5.1 and 5.2. We adopt

$$R_M = \frac{R_{M0}}{1 + c_1 R_{M0} (B_{rms}^2)}, \quad \alpha = \alpha_0 (1 + c_2 B_{rms}^2). \quad (5.3)$$

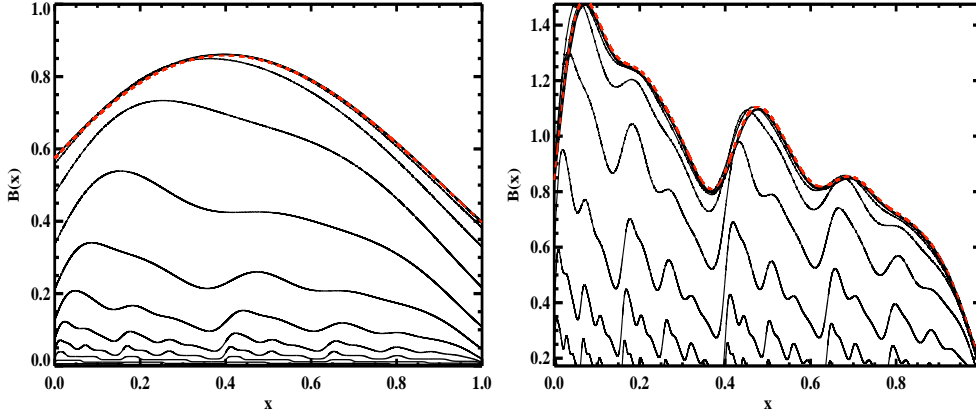


FIGURE 13. The nonlinear evolution of the eigenfunctions of the 2-strip map, due to saturation by combining both increased diffusion and reduced stretching, adopting initial  $\alpha_0 = 0.4$  and  $R_M = 10^5$ . The left panel shows the result of adopting  $c_1 = 0.1$  and  $c_2 = 0.9$  (case A), while the right shows the case when  $c_1 = 0.001$  and  $c_2 = 0.999$  (case B). The effective magnetic Reynolds number at saturation is  $R_{\text{sat}} = 18$  and  $R_{\text{sat}} = 1066$ , for case A and B respectively. The corresponding kinematic eigenfunctions are shown as dashed lines in the figure. We see that the shape of  $B(x)$  at saturation closely matches that of the kinematic eigenfunction for  $R_M = R_{\text{sat}}$ .

For  $c_1 = 1$  and  $c_2 = 0$  we have saturation purely by the nonlinear decrease of  $R_M$ , while  $c_1 = 0$  and  $c_2 = 1$  corresponds to the case when saturation occurs purely due to reduced stretching. We consider now the intermediate case where both  $c_1$  and  $c_2$  are non zero.

The evolution of  $B(x, t)$  of the 2-strip map, adopting initial  $\alpha_0 = 0.4$  and  $R_{M0} = 10^5$  is shown in Fig. 13, for two cases. The left panel shows the result of adopting  $c_1 = 0.1$  and  $c_2 = 0.9$  (case A), while the right shows the case when  $c_1 = 0.001$  and  $c_2 = 0.999$  (case B). The effective magnetic Reynolds numbers at saturation have now reduced from  $R_{M0} = 10^5$  to  $R_M = R_{\text{sat}} = 18$  and  $R_M = R_{\text{sat}} = 1066$ , for cases A and B respectively. The corresponding kinematic eigenfunctions are shown as dashed lines in the figure. Remarkably, we see from Fig. 13 that the the shape of  $B(x)$  at saturation for both cases, now closely matches that of the corresponding kinematic eigenfunction for  $R_M = R_{\text{sat}}$ . Thus when both the effective diffusion of the field and the stretching efficiency are affected by Lorentz forces, as would perhaps be most realistic, then the dynamo saturates with an intermediate spatial structure; that of the kinematic eigenfunction with  $R_M = R_{\text{sat}}$  with  $R_{M0} > R_{\text{sat}} > R_{\text{crit}}$ .  $R_{\text{sat}}$  is determined by the relative importance of the increased diffusion versus the reduced stretching. However a change in  $c_1$  has a more dramatic effect than an equal change in  $c_2$ , as  $c_1$  appears in an exponential function, the Gaussian in Eq. 3.7 involved in convolution to incorporate resistive effects.

## 6. Conclusions

We have explored here the evolution and saturation behaviour of map dynamos used by Finn & Ott (1988, 1990) to model Zeldovich's STF dynamo. One of our aims is to use these simpler systems to develop some intuitive understanding of the saturation behaviour of more realistic fluctuation dynamos. The use of maps also allows one to analyze dynamos with very high values of  $R_M$ , much higher than what can be achieved in DNS.

We have considered in particular two types of the generalized Baker's maps, the 2-strip

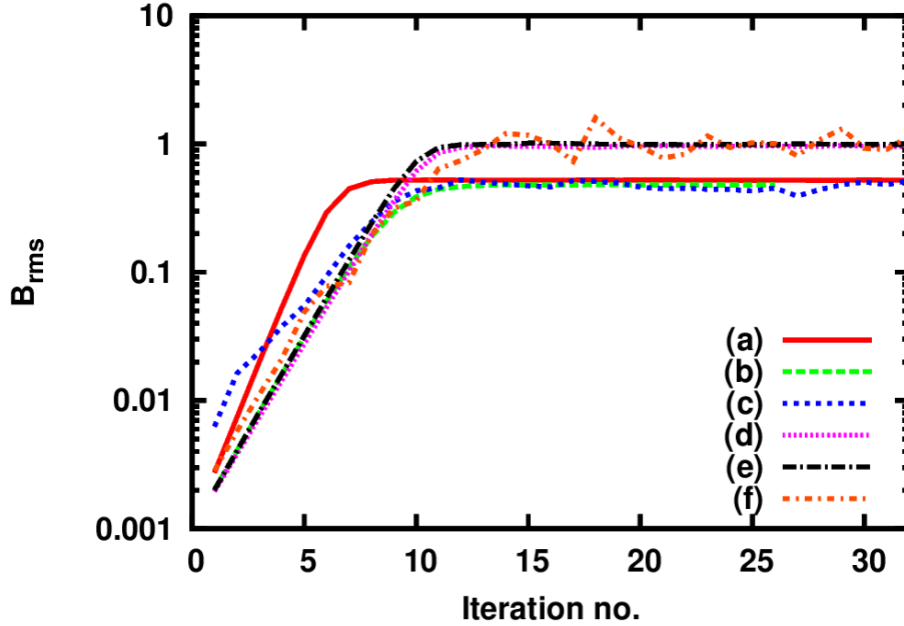


FIGURE 14. Comparison of  $B_{rms}$  for various cases. (a): 2 strip map with  $R_M = 1000$ , saturation by decreasing  $R_M$ , (b): 2 strip map with  $R_M = 10^4$ , saturation by decreasing  $R_M$ , (c): 4 strip map with  $R_M = 10^5$ , saturation by decreasing  $R_M$ , (d): 2 strip map with  $R_M = 1000$ , saturation by decreasing stretching, (e): 2 strip map with  $R_M = 10^4$ , saturation by decreasing stretching, (f): 4 strip map with  $R_M = 1000$ , saturation by decreasing stretching

map where there is constant constructive folding and the 4-strip map which allows the possibility of reversal of the field. In the absence of diffusion, the magnetic field  $B(x)$  generated by the map dynamo develop a fractal structure (Finn & Ott 1988, 1990). On including a diffusive step in the map, parameterised by the magnetic Reynolds number  $R_M$ , we find that the magnetic field  $B(x)$  is amplified only above a critical  $R_M = R_{crit} \sim 4$  for both types of dynamos. The spatial structure of the growing  $B(x)$  also becomes shape invariant (with iteration number), corresponding to an eigenfunction of the map dynamo, but whose complexity increases with increasing  $R_M$ . The kinematic eigenfunction of the 4-strip map shows reversals of the field, whose number increases with  $R_M$ . These results are similar to those presented in Finn & Ott (1988, 1990) on the kinematic stage of the map dynamos.

We then explored different ways by which the STF map dynamos could saturate. Saturation can occur due to a renormalized increase of the effective resistivity or by decreasing  $R_M$ . Such an effect obtains in a model where the Lorentz forces leads to a ‘ambipolar’-type nonlinear drift velocity (Subramanian 1999). For both the 2-strip map and the 4-strip map which includes field reversals,  $B(x)$  in the saturated state goes back to the marginal eigenfunction, which would obtain for the critical  $R_M = R_{crit}$ . The structure developed during the kinematic stage is lost on saturation and thus one can conclude that the energy is being effectively transferred to the larger scales due to non-linear evolution, analogous to the analytical results of Subramanian (1999) and the DNS results of Haugen *et al.* (2004); Eyink *et al.* (2013); Bhat & Subramanian (2013) for fluctuation dynamos with  $P_M = 1$ .

We have also explored the saturation of the dynamo, when the effect of Lorentz forces is to decrease the efficiency of field amplification by stretching. For the 2-strip map, we

show that  $B(x)$  now saturates preserving the structure of the kinematic eigenfunction got using the initial  $R_M = R_{M0}$ . Thus energy is still preserved at the smallest scales which survive resistive diffusion. This is analogous to the results of Schekochihin *et al.* (2004) for the large  $P_M$  and small  $Re$  fluctuation dynamo, where power on resistive scales appear to be preserved during saturation. However an intermediate behaviour obtains when both saturation mechanisms operate in tandem. The saturated  $B(x)$  has now the spatial structure of kinematic eigenfunction with an intermediate  $R_M = R_{\text{sat}}$  where  $R_{M0} > R_{\text{sat}} > R_{\text{crit}}$ . Even a small increase in the effective diffusion with growing field, (with  $c_1 \ll 1$ ) significantly smoothens the spatial structure of the field. For the 4-strip map, saturation due to decreased stretching efficiency leads to a more complicated behaviour, as now the saturated  $B(x)$  oscillates with time, although with a structure similar to the kinematic eigenfunction.

One could have naively expected that  $B(x)$  is driven to a universal form on saturation. However, it appears that the field structure when dynamos saturate is a nontrivial issue even for the simple map dynamos, and depends on the exact manner of saturation. The two natural possibilities, that the saturated eigenfunction approaches the marginal eigenfunction or remains of the same form as the kinematic eigenfunction, are both realized for different modes of saturation. If one takes a hint from such map dynamos, then even for the fluctuation dynamo in a random flow, the structure of the saturated state could depend on the control parameters of the system, like  $R_M$ ,  $Re$  and  $R_{\text{crit}}$ . It would be interesting to explore such issues further. It would also be interesting to extend the map dynamos to incorporate a range of length scales, so as to mimic more realistically a turbulent flow with a range of eddy scales, and study their saturation behaviour.

## Acknowledgments

AS thanks IUCAA for hospitality during his visits there under the Visiting Student Programme. PB acknowledges support from CSIR. We acknowledge the use of the high performance computing facility at IUCAA.

## REFERENCES

- BERNET, M. L., MINIATI, F., LILLY, S. J., KRONBERG, P. P. & DESSAUGES-ZAVADSKY, M. 2008 Strong magnetic fields in normal galaxies at high redshift. *Natur* **454**, 302–304.
- BHAT, P. & SUBRAMANIAN, K. 2013 Fluctuation dynamos and their Faraday rotation signatures. *MNRAS* **429**, 2469–2481.
- BHAT, P. & SUBRAMANIAN, K. 2014 Fluctuation Dynamo at Finite Correlation Times and the Kazantsev Spectrum. *ApJ* **791**, L34.
- BRANDENBURG, A., SOKOLOFF, D. & SUBRAMANIAN, K. 2012 Current Status of Turbulent Dynamo Theory. From Large-Scale to Small-Scale Dynamos. *SSRv* **169**, 123–157.
- BRANDENBURG, A. & SUBRAMANIAN, K. 2005 Astrophysical magnetic fields and nonlinear dynamo theory. *PhR* **417**, 1–209.
- CHILDRESS, S. & GILBERT, A. D. 1995 *Stretch, Twist, Fold*.
- CHO, J. & RYU, D. 2009 Characteristic Lengths of Magnetic Field in Magnetohydrodynamic Turbulence. *ApJ* **705**, L90–L94.
- CLARKE, T. E. 2004 Faraday Rotation Observations of Magnetic Fields in Galaxy Clusters. *Journal of Korean Astronomical Society* **37**, 337–342.
- CLARKE, T. E., KRONBERG, P. P. & BÖHRINGER, H. 2001 A New Radio-X-Ray Probe of Galaxy Cluster Magnetic Fields. *ApJ* **547**, L111–L114.
- ENSSLIN, T. A. & VOGT, C. 2006 Magnetic turbulence in cool cores of galaxy clusters. *A&A* **453**, 447–458.
- EYINK, G., VISHNIAC, E., LALESCU, C., ALUIE, H., KANOV, K., BÜRGER, K., BURNS, R.,

- MENEVEAU, C. & SZALAY, A. 2013 Flux-freezing breakdown in high-conductivity magnetohydrodynamic turbulence. *Natur* **497**, 466–469.
- EYINK, G. L. 2011 Stochastic flux freezing and magnetic dynamo. *PRE* **83** (5), 056405.
- FINN, J. M. & OTT, E. 1988 Chaotic flows and magnetic dynamos. *Physical Review Letters* **60**, 760–763.
- FINN, J. M. & OTT, E. 1990 The fast kinematic magnetic dynamo and the dissipationless limit. *Physics of Fluids B* **2**, 916–926.
- HAUGEN, N. E., BRANDENBURG, A. & DOBLER, W. 2004 Simulations of nonhelical hydromagnetic turbulence. *PRE* **70** (1), 016308.
- HAUGEN, N. E. L., BRANDENBURG, A. & DOBLER, W. 2003 Is Nonhelical Hydromagnetic Turbulence Peaked at Small Scales? *ApJ* **597**, L141–L144.
- KAZANTSEV, A. P. 1968 Enhancement of a Magnetic Field by a Conducting Fluid. *Soviet Journal of Experimental and Theoretical Physics* **26**, 1031.
- SCHEKOCHIHIN, A. A. & COWLEY, S. C. 2006 Turbulence, magnetic fields, and plasma physics in clusters of galaxies. *Physics of Plasmas* **13** (5), 056501.
- SCHEKOCHIHIN, A. A., COWLEY, S. C., TAYLOR, S. F., MARON, J. L. & MCWILLIAMS, J. C. 2004 Simulations of the Small-Scale Turbulent Dynamo. *ApJ* **612**, 276–307.
- SUBRAMANIAN, K. 1999 Unified Treatment of Small- and Large-Scale Dynamos in Helical Turbulence. *Physical Review Letters* **83**, 2957–2960.
- SUBRAMANIAN, K., SHUKUROV, A. & HAUGEN, N. E. L. 2006 Evolving turbulence and magnetic fields in galaxy clusters. *MNRAS* **366**, 1437–1454.
- TOBIAS, S. M., CATTANEO, F. & BOLDYREV, S. 2011 MHD Dynamos and Turbulence. *ArXiv e-prints* .
- VAINSHTEIN, S. I. & ZEL'DOVICH, Y. B. 1972 REVIEWS OF TOPICAL PROBLEMS: Origin of Magnetic Fields in Astrophysics (Turbulent "Dynamo" Mechanisms). *Soviet Physics Uspekhi* **15**, 159–172.
- ZELDOVICH, I. B., RUZMAIKIN, A. A. & SOKOLOV, D. D., ed. 1983 *Magnetic fields in astrophysics*, , vol. 3.